CAMERA SELF-CALIBRATION BY USING SfM BASED DENSE MATCHING FOR CLOSE-RANGE IMAGES

Cihan Altuntaş [1,*] iD

[1] *Konya Technical University, Faculty of Engineering and Natural Sciences, Selcuklu, Konya, Turkey*
Corresponding author: C. Altuntas (caltuntas@ktun.edu.tr).

ABSTRACT

The camera calibration is an important issue that must be overcome to getting metric scene measurement. The imaging parameters are estimated by calibration of the camera. Basically, the camera calibration is performed individually from the photogrammetric evaluation. Today, 3-D point cloud generation and the camera calibration are usually attained simultaneously by using SfM approach photogrammetric evaluation. Stereo images that do not have camera intrinsic parameters can also be evaluated by SfM based photogrammetry. In this study, camera calibration models were investigated for point cloud generation of close-range photogrammetry. The results shown that self-calibration of loop-close images enables the close results to the pre-calibration. Otherwise, the images should be convergent as far as possible or projection-to-sparse point cloud ratio must be raised. The results show that the projection-to-sparse point cloud ratio of 13.22 created high accuracy to self-calibration. Consequently, the pre-calibration requires extra computation and time. However the self-calibration can be implemented for high accuracy measurement subject to convergence imaging or sufficient number of projection.

Keywords: Camera calibration, Dense matching, Image matching, Self-calibration, Point cloud.

1. INTRODUCTION

Three-dimensional (3-D) measurement is prevalent task in many disciplines for the aim of 3-D modelling and visualization. The users are benefited from different instrument and techniques to carry out the operation. The photogrammetry is highly accurate and low-cost method for terrestrial 3-D measurement. Many innovations in computer vision have been adopted to photogrammetry for acquire more dense measurement data in a short time. The photogrammetry uses structure-from-motion (SfM) based on automatic measurement [1, 2]. It extracts measurement data from metric or non-metric camera images. Any source of overlapping images [3] or imageries [4] can be evaluated with SfM based photogrammetry for generating high density 3D measurement data.

The SfM matches unordered overlapping images automatically without camera calibration data [5]. After the image keypoints (feature points) which does not change with respect to perspective, scale and orientation of the image are detected, they are matched with their similarities. The number of matched keypoints affects the measurement accuracy from stereo images of photogrammetry [6]. The images should have perspective projection and, any deviations from the perspective projection must be modelled as mathematically for high accuracy from the photogrammetric evaluation [7]. The deviation from the perspective projection is called as distortion and it can be removed from the images by using the camera calibration parameters. Thus the calibration parameters of the camera must be known for right spatial measurement from the photogrammetry. The images, which have the camera calibration parameters, are called metric, non-metric otherwise. The camera calibration performed with the special test field before the photogrammetric measurement is named pre-calibration. The pre-calibration requires to design a special test field with location known control points. It is time and labour consuming task. The camera calibration which is performed together with object images on the photogrammetric evaluation is called as self-calibration [8]. The images are matched as automatically by using SfM algorithm and the calibration parameters are estimated with photogrammetric bundle adjustment in the self-calibration. This study investigates the camera calibration methods and its relation to photogrammetric measurement accuracy.

The camera convergence and number of projection must be in proper one to performing correct self-calibration and 3-D measurement from SfM based photogrammetry. The pre-calibration enables high accuracy to photogrammetric measurement [9,10]. However, professional or usually non-professional applicants prefer to self-calibration based photogrammetric measurement since its easy, practical and has very fast applications. The SfM gives rise to generation high accuracy self-calibration parameters and measurement data with depends on imaging surface geometry.

In earlier 3-D measurement studies, 0.2 mm accuracy could be achieved from photogrammetry by using self-calibration of non-metric cameras [11]. The high accuracy makes enable to the close-range photogrammetry to use in earth surface deformation [12] and industrial measurement [13]. The smart phone stereo images have also been used for photogrammetric

C. Altuntaş

measurement. The calibrated smart phone cameras exhibited lower accuracy than the metric cameras, but the results were relatively satisfactory in comparison to studies using other inexpensive cameras [14]. [10] shown that the incorporation of dGPS supported control points (CPs) and a pre-calibrated camera model can result in systematic distortion being reduced to below detection levels. Nevertheless the commercial softwares do not provide a one-size-fits-all solution to getting high accuracy from pre- or self- calibration and workflows should be adjusted so to topography. In this study SfM based point cloud generation workflow for non-, pre- and self- calibrated camera images were investigated. The self-calibration is highly related to image convergence and number of corresponding points between the overlapping images. The self-calibration was performed with different image configurations related to convergence and projection numbers. The distortions and CP residuals were compared for accuracy evaluations.

2. METHODOLOGY

2.1. Stereo-view Measurement

The close-range photogrammetry has interdisciplinary characters with its varied applications [12,13,15,16]. Its industrial applications have 0.1 mm measurement accuracy, and the accuracy varies around 1 cm for large-scale object measurement. The measurement accuracy changes with respect to applied evaluation model, imaging properties (metric or non-metric), image scale and ground sapling distance (GSD).

The main purpose of a photogrammetric measurement is the 3-D reconstruction of an object in digital form with coordinates or wireframe geometric elements. The measurement data are generated from overlapping area of a stereo image that has central projection properties. The 3-D visualization is acquired from stereo images by imitating the human eye interpretation. The photogrammetric evaluation is performed basically in three steps such as inner, relative and absolute orientations.

At the inner orientation, image generation optical properties that were estimated by the camera calibration are implemented to photogrammetric evaluation. These optical values which are called camera intrinsic parameters are focal length *f*, principal point (PP) coordinates (x_o, y_o) and pixel dimensions (Figure 1). The principle point is defined as the image points where the optical axis intersects with the image plane. Its image coordinates are estimated by calibration of the camera.
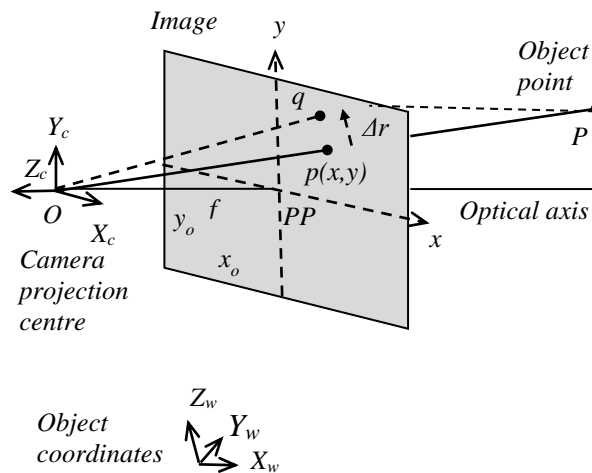

Figure 1. The camera imaging geometry and distortion error

The 3-D visualization from stereo images is getting via relative orientation by applying the co-planarity constraint. The relationship between the camera projection centre 0, image point *p* and object point *P* are expressed well-known colinearity model in perspective transformation (Eq. 1).

$$\begin{pmatrix} x - x_o + \Delta x \\ y - y_o + \Delta y \\ -f \end{pmatrix} = \lambda R \begin{pmatrix} X_w - X_w^c \\ Y_w - Y_w^c \\ Z_w - Z_w^c \end{pmatrix} \tag{1}$$

CAMERA SELF-CALIBRATION BY USING SfM BASED DENSE MATCHING FOR CLOSE-RANGE IMAGES

Where; *x,y* are image coordinates; X_w, Y_w, Z_w are object coordinates; X_w^o, Y_w^o, Z_w^o are the place of the projection centre and *R* is rotation matrix (3x3 dimensions). The additional parameters Δx and Δy are account distortions from colinearity condition. The colinearity condition for all the object points must be realized in every images of the stereo view for 3-D visualization. In this way, the projection centres, object points and its image points are lie on the same plane (Figure 2). This geometrical condition in photogrammetry is named as co-planarity constraint for the stereo-view. It is realized to relative orientation and translation of the images with respect to each other. It has five unknown parameters which are estimated with least five conjugate points. The relative orientation provides 3-D object model at unknown arbitrary scale. The scale has been attained to the model with the absolute orientation.
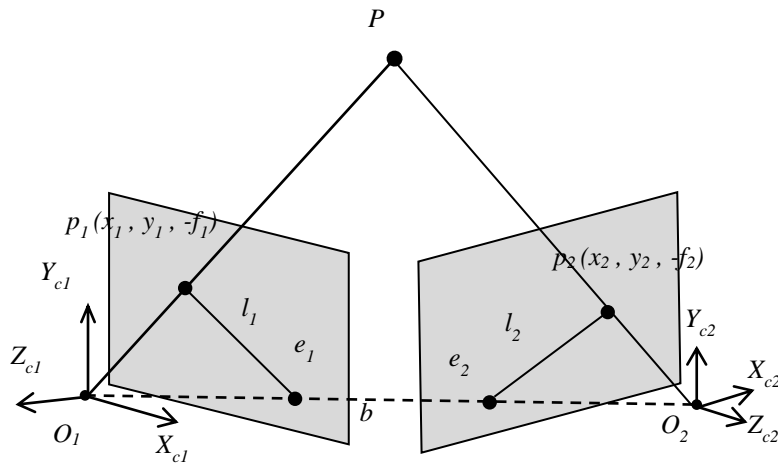

Figure 2. The epipolar geometry

2.2. Camera Calibration

The camera calibration covers the estimation of intrinsic and distortion parameters. It is an active research topic in geomatics and computer science community to get high accuracy from the photogrammetry. The automatic calibration methods had been applied to digital cameras with colour code or special shape targets in the literature [17,18]. Moreover the validity of calibration data over a time should be carefully assessed before next photogrammetric measurement [19].

The calibration models are classified into two categories such as linear and non-linear [7,20]. The linear models, i.e. Hall and Faugeras–Toscani, use a least-squares technique to get the parameters of the model [21-24]. Non-linear calibrating methods as with Faugeras with distortion, Tsai and Weng, use a two-stages as a linear approximation and then iterative algorithm to optimize the parameters [25-28].

The camera calibration is outperformed by using single or multi-view perspective images. The extensive approach for a single image camera calibration is to adopt vanishing points and vanishing lines [29,30]. It can be applied with and without any special calibration pattern [31]. The multi-view calibration is applied with many images from different perspectives of the same imaging area by applying linear or non-linear methods.
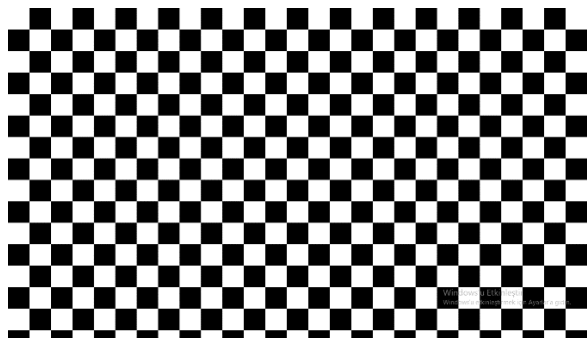

Figure 3. Test grid on computer screen for Agisoft Lens

The calibration is performed with the special test area which has target points localized in 2-D (Figure 3) or 3-D space. The line segmentation has also been used to match multi-view images for the calibration [32,33]. However the point based calibration is popular in multi-view photogrammetry [34]. The point based method is, in addition, applied for a single image camera calibration [35]. The point based calibration method usually use special target shape for automatic detection, and is exploited in pre-calibration of the camera. The pre-calibration can be performed with manually selected target points also.

The SfM based automatic image matching have created an opportunity for the camera calibration by using images of a survey object [10,36,37]. The colinearity condition enables that the camera calibration can be performed together with the object measurement using the bundle adjustment evaluation model. This calibration model of the camera is called as self-calibration. Theoretically known and unknown intrinsic parameters of the camera show the necessary camera numbers for the calibration. The most popular approach is only focal lengths to be unknown and varying, and all the other parameters to be known [38]. Number of counting argument gives a necessary condition for self-calibration. If it is assumed as m the number of cameras, n_k the number of known internal parameters, and n_f the number of constant (but unknown) internal parameters, a necessary condition is given [9] by

$$mn_k + (m-1)n_f \geq 8 \tag{2}$$

In Eq. (2), when $n_k=3$ (focal length and principal point coordinates) and $n_f=0$, m must be three or more. The number of unknown parameters to inner orientation and distortion are eight for non-metric images, and require least eight images to estimation all of these parameters. Accordingly, full calibration could not be procured with the self-calibration from two-view stereo images.

2.3. Distortion Error

The image distortions must be corrected as mathematically to getting high accuracy from the photogrammetric measurement. Δx and Δy include colinearity condition's physical departures such as symmetric radial distortion (Δr), decentring (tangential) distortion (Δd), image plane unflatness (Δu) and in-plane image distortion (Δf) [39].

$$\Delta x = \Delta x_r + \Delta x_d + \Delta x_u + \Delta x_f \tag{3}$$

$$\Delta y = \Delta y_r + \Delta y_d + \Delta y_u + \Delta y_f \tag{4}$$

The net image displacement at any point will amount to the cumulative influence of each perturbations in Eq (3) and Eq (4). The effect of tangential, unflatness and in-plane distortions are so small and insignificant magnitude in these perturbations and are not taken into account in CCD or CMOS relevant digital images. The radial lens distortion has usually large effect in digital images.

Radial lens distortion has symmetric effect according to the principal point. It is represented as polynomial Eq. (5);

$$\Delta r = K_1 r^3 + K_2 r^5 + K_3 r^7 \tag{5}$$

Where; K_i terms are the coefficients of radial distortion and r is the radial distance from the principal point. The perturbation related to radial distortion is increasing according to radial distance r and it reaches largest at the border of the image. K_1 term suffice for medium level accuracy in photogrammetric measurement. K_2 and K_3 coefficients improve the accuracy.

The related correction to the *x,y* image coordinates are proportional to their magnitude (Eq. 6)

$$\Delta x_r = \bar{x}\frac{\Delta r}{r} \qquad and \qquad \Delta y_r = \bar{y}\frac{\Delta r}{r} \tag{6}$$

$$r = \sqrt{\bar{x}^2 + \bar{y}^2} \tag{7}$$

Then distortion corrected image coordinates are obtained by Eq (8)

$$x = \bar{x} + \Delta x_r \qquad and \qquad y = \bar{y} + \Delta y_r \tag{8}$$

Tangential distortion are given by Eq (9)

$$\Delta d = r^2\sqrt{P_1^2 + P_2^2} \tag{9}$$

CAMERA SELF-CALIBRATION BY USING SfM BASED DENSE MATCHING FOR CLOSE-RANGE IMAGES

Where; P_1 and P_2 are the coefficients of tangential distortion. Tangential distortion rarely exceeds 10 micron as determined in a self-calibration. The resulting image coordinate perturbations are very small and the distortion variation is generally ignored in photogrammetry. Out-of-plane distortion occurs due to unflatness of sensor surface and reaches highest one or two micron height differences in sensor surface. In-plane image distortion expresses orthogonality (shear) and scale differences between the sensor pixels on rows and columns [39].

2.4. Essential and Fundamental Matrix

The Essential (E) and Fundamental (F) matrices have 3x3 dimensions that represent the epipolar geometry between stereo images. They indicate epipolar line to search along in the second image for given a point in the first image (Figure 2). The E matrix had been introduced first and then F matrix [40]. The F matrix is generalization of the E matrix in which the calibrated camera is removed. The E matrix has fewer degrees of freedom compared to F matrix.

If the camera is pre-calibrated, the SfM uses E matrix to search possible match point in the other image, otherwise F matrix is exploited to SfM. The E matrix uses extrinsic camera parameters while the F matrix uses both intrinsic and extrinsic camera parameters in this task. In other words, E matrix uses camera coordinates while F matrix is using the image coordinates for matching the image points.

After the principal point offset and camera-specific distortions are corrected, the relationship between corresponding points p_1 (x_1, y_1, $-f_1$) and p_2 (x_2, y_2, $-f_2$) is described with E matrix given by Eq (10).

$$p_2^T E p_1 = 0 \tag{10}$$

$$\det E = 0 \tag{11}$$

The E matrix has five degrees of freedom and incorporated within a RANSAC procedure for deriving exterior orientation parameters of the stereo images. It is estimated with eight point correspondences with constraint $e^T e = 1$ and its singular value decomposition (SVD). E matrix uses normalized image coordinates.

The F matrix, that comprises both intrinsic and extrinsic camera parameters, connects two corresponding points from the stereo images as Eq (12)

$$p_2^T F p_1 = 0 \tag{12}$$

$$\det F = 0 \tag{13}$$

F matrix has nine degrees of freedom and estimated with eight point correspondences [9]. It also is incorporated within RANSAC procedure for solving the correspondence problem between the stereo images.

2.5. Point Cloud Generation

The self-calibration cannot be performed with a photogrammetric evaluation of two-view stereo images. Two-view photogrammetric measurement is executed as pre-calibration or without calibration parameters (as non-metric) of the images (Figure 4).

The keypoints are detected by feature point operators such as SIFT [41]. The SfM approach generates tie points between overlapping images by matching the possible candidate keypoints as automatically. The sparse point cloud is generated by estimating the object coordinates of these tie points. The SfM estimates order and orientation of the cameras with respect to unknown local coordinates. The self-calibration is performed with bundle adjustment of multi-view (least 3 views) stereo images. The known intrinsic and distortion parameters can be excluded from the self-calibration. Thereby, a multi-view photogrammetric evaluation is executed as metric images with pre-calibration. In addition, multi-view photogrammetric evaluation can also be executed to non-metric (without calibration) images (Figure 5).
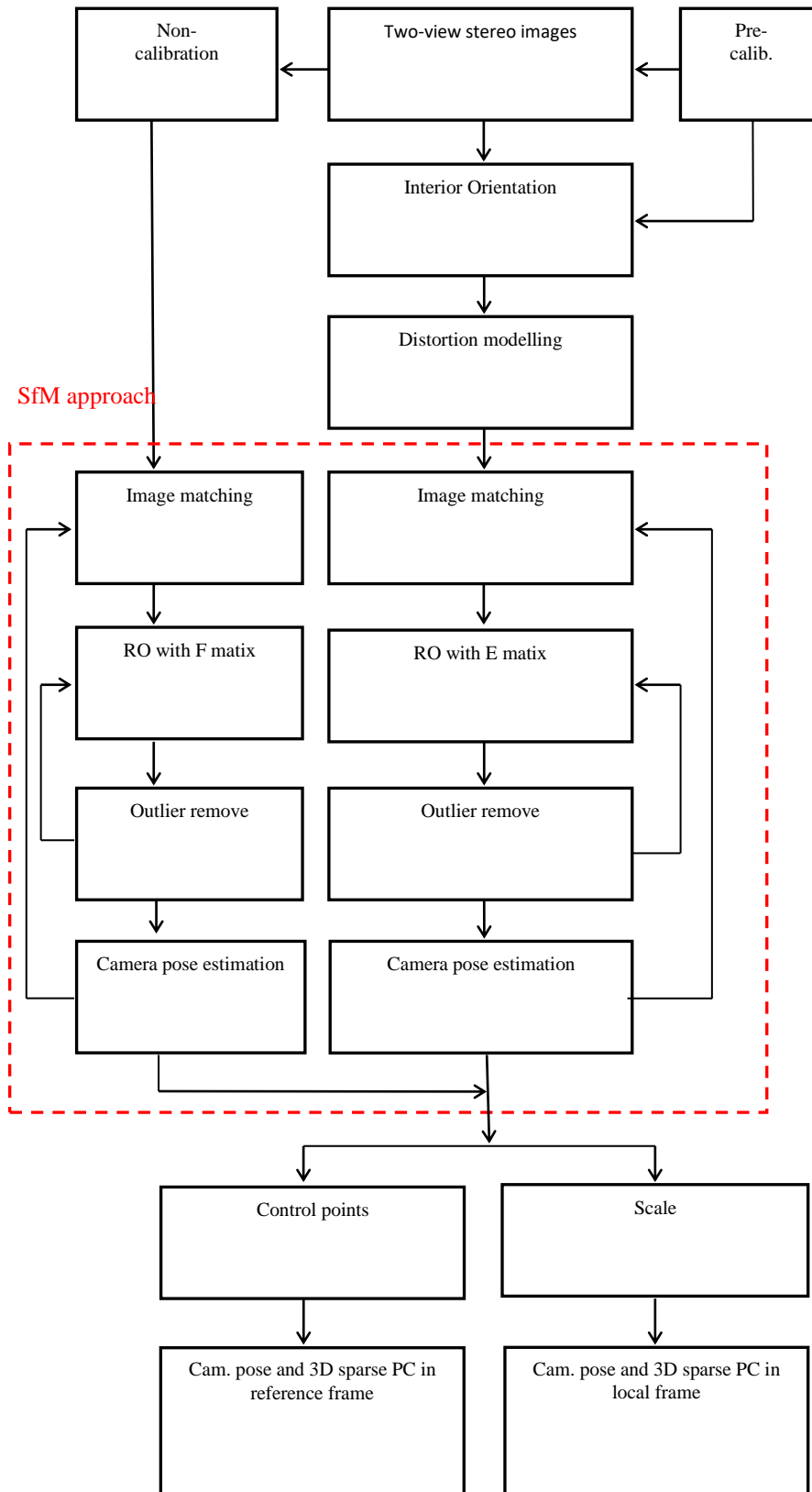
Figure 4. The workflow of SfM based photogrammetric evaluation of two view stereo images. The camera self-calibration is not possible for two view images.

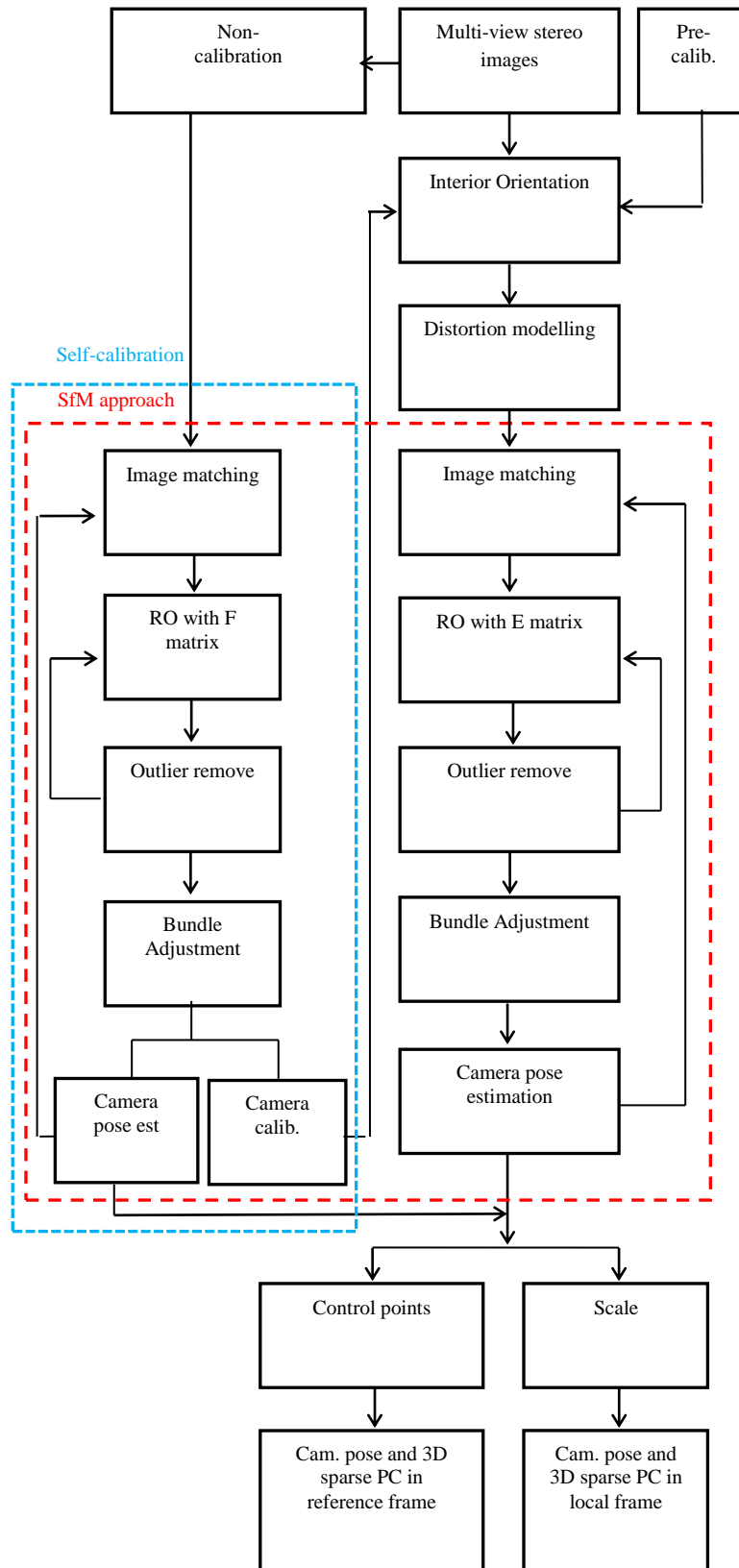*CAMERA SELF-CALIBRATION BY USING SfM BASED DENSE MATCHING FOR CLOSE-RANGE IMAGES*

Figure 5. The workflow of SfM based photogrammetric evaluation of multi-view stereo images. The camera self-calibration parameters can also be estimated in multi-view evaluation. The estimated camera calibration parameters can be applied to again evaluation.

C. Altuntaş

3. RESULTS

3.1. Pre-Calibration

The pre-calibration is usually performed with special design test field which has control points with known target shape. The Agisoft lens software uses chessboard plane to do pre-calibration (Figure 3). The chessboard is shown on computer screen and nine convergent images are recorded from different point of view. The images are matched automatically and the calibration parameters are estimated with bundle adjustment. The estimated camera intrinsic parameters and distortion graphics are given on Table 1 and Figure 6.

Table 1. Agisoft Lens pre-calibration results of Nikon P50 camera (3264x2448 pixel array)

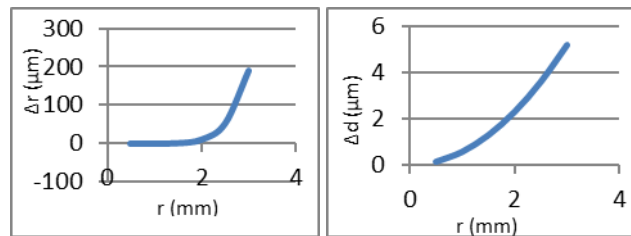| Parameters	Quantitate
f (pixel)	2700.220
x_o (pixel)	1604.060
y_o (pixel)	1229.040
Radial K_1	-0.111631000
Radial K_2	-0.002199310
Radial K_3	0.088830800
Tangential P_1	-0.000520235
Tangential P_2	0.000246494
b_1	-0.556039
b_2	0.337776

Figure 6. The radial and tangential distortion for pre-calibration of Nikon P50 camera

3.2. Convergent Related Self-Calibration

The convergent angle and related base-to-height ratio effect the accuracy of photogrammetric measurement. The large convergent angle, that base-to-height ratio is around 1.5, increases the measurement accuracy. The multi-image camera geometry is, as a rule, guaranty measurement accuracy that comprised base-to-height ratio. However the convergent degrees of the images also affect the accuracy, especially in structure measurement with loop close or loop open image configurations. The camera self-calibration and measurement were tested on a historical mosque. The structure has roughly rectangular shape in 37x47 m^2 dimensions. The images were collected by Nikon P50 camera as partially overlapping from 14.7 m distance away in ground resolution of 5.42 mm/pixel. The image based point cloud measurement data were generated as loop close and various convergence degree images as loop open configurations. The loop open convergence images were evaluated with four configurations as four, three, two and one (line) façades (Figure 7). The self-calibration that includes camera intrinsic and distortion parameters were carried out together with the estimation of tie point object coordinates by applying multi-image bundle adjustment (Table 2, Figure 8). The point cloud based on bundle adjustment was, also, created using the camera pre-calibration and without calibration as non-metric images. As mentioned above the epipolar constraint was applied to stereo images using E and F matrix for metric and non-metric images respectively. The measurement accuracy was evaluated with the residuals between measured and estimated coordinates of the CPs (Table 3).

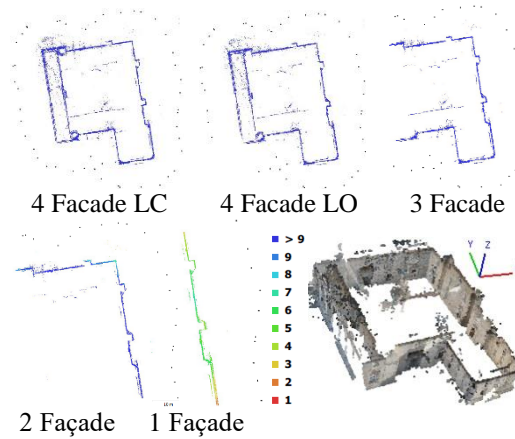*CAMERA SELF-CALIBRATION BY USING SfM BASED DENSE MATCHING FOR CLOSE-RANGE IMAGES*

Figure 7. The different level convergence imaging for multi-image photogrammetric measurement. (Colour legend shows number of overlapping images)

Table 2. The estimated interior parameters relation to convergence images

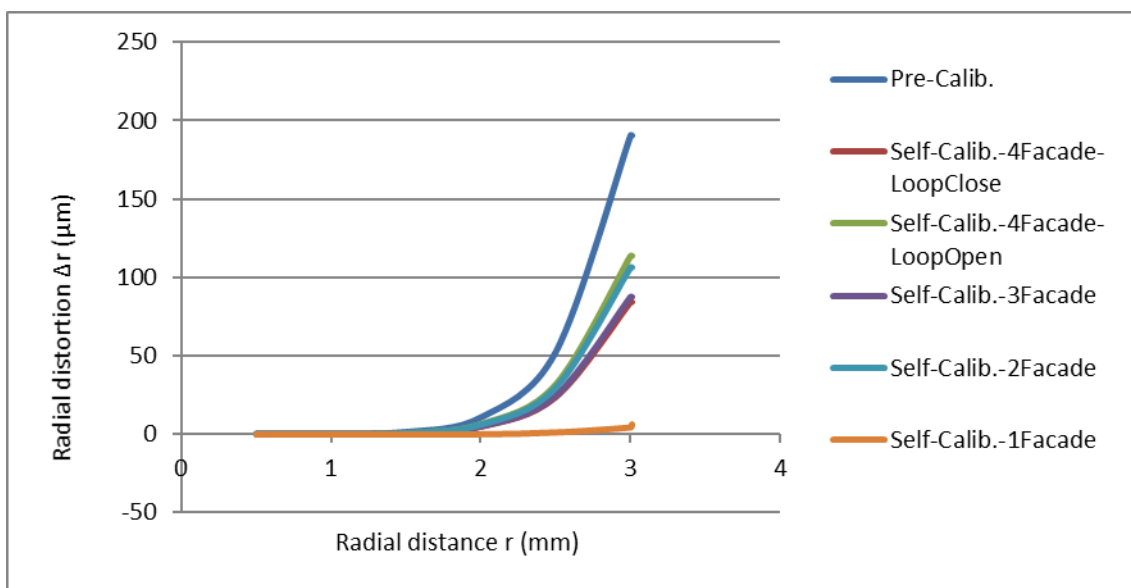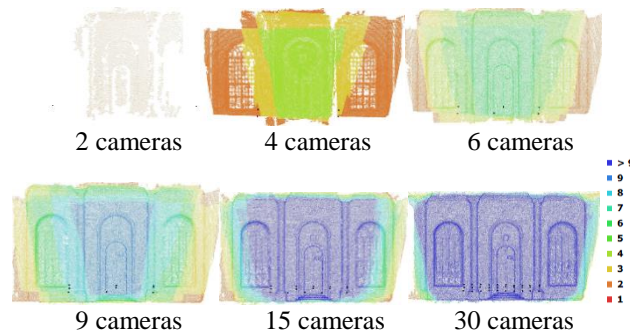| Calibration	f (pixel)	x_o (pixel)	y_o (pixel)
Pre-	2700.220	-27.935	5.042
Self- 4Facade-LoopClose	2700.370	-22.157	5.826
Self- 4Facade-LoopOpen	2703.950	-23.281	6.788
Self- 3Facade	2705.320	-18.102	3.358
Self- 2Facade	2704.410	-20.378	8.107
Self- 1Facade	2702.730	-18.465	10.141

Figure 8. Image convergences and related radial distortions for pre- and self- calibrations

C. Altuntaş

Table 3. The building convergence images and point cloud generation from pre- self- and non- calibrated images

Façade#	Calibration	CP#	RMSE_ XYZ (cm)	Image#	Sparse Point (SP)#	Projection#	Projection# /SP#	Projection# /Image#
4 Façade- Loop close- Convergent	Pre-	8	0.86	50	67223	161607	2.40	3232
	Self-		0.68					
	Non-		14.30					
4 Façade- Loop open- Convergent	Pre-	8	0.68	46	61543	148256	2.41	3223
	Self-		0.32					
	Non-		15.38					
3 Façade- Convergent	Pre-	6	0.72	36	47722	116708	2.44	3242
	Self-		0.35					
	Non-		14.44					
2 Façade- Convergent	Pre-	4	0.66	22	30546	75692	2.48	3441
	Self-		0.23					
	Non-		19.71					
1 Façade- Plane	Pre-	3	0.53	11	15418	35534	2.30	3230
	Self-		0.08					
	Non-		25.49					

3.3. Projection Related Self-Calibration

The experiments were made on façade (22x12 m2 dimensions) of a historical structure. Thirty images were recorded from the structure façade as regular space projection centres in overlapping positions. The images were taken 13.7 m distance away from the object surface (Figure 9). The scale is around 3028 and, ground resolution is 5.06 mm/pixel for all the images.

2 cameras   4 cameras   6 cameras

9 cameras   15 cameras   30 cameras

Figure 9. Camera stations and point projections (Colour legend shows number of overlapping images and projections as well)

Table 4. The pre- and self- calibration interior parameters for different number multi-view images

Calibration	f (pixel)	x_o (pixel)	y_o (pixel)
Pre-	2700.220	-27.935	5.042
Self-30 cameras	2702.770	-23.229	1.793
Self-15 cameras	2705.660	-23.432	0.385
Self-9 cameras	2700.370	-21.481	-0.975
Self-6 cameras	2703.980	-22.548	-3.661
Self-4 cameras	2710.590	-31.625	-5.614

CAMERA SELF-CALIBRATION BY USING SfM BASED DENSE MATCHING FOR CLOSE-RANGE IMAGES

The image based point cloud data can be created from two-view or multi-view stereo images using SfM approach. However, self-calibration data can be estimated only for multi-view photogrammetric evaluation of partially overlapping three or more images. Every extra image to the evaluated image block increases the accuracy of point projection and measurement. A projection number of any connected point indicates that how many images are covering and connected to this point. The self-calibration and point cloud creation were performed with the varying number of images. The self-calibration parameters were estimated for image sets of 4, 6, 9, 15 and 30 cameras (Table 4, Figure 10). The image blocks are, also, evaluated with the pre-calibration as metric images and without calibration as non-metric images. The measurement accuracy was evaluated with the residuals on the CPs (Table 5).
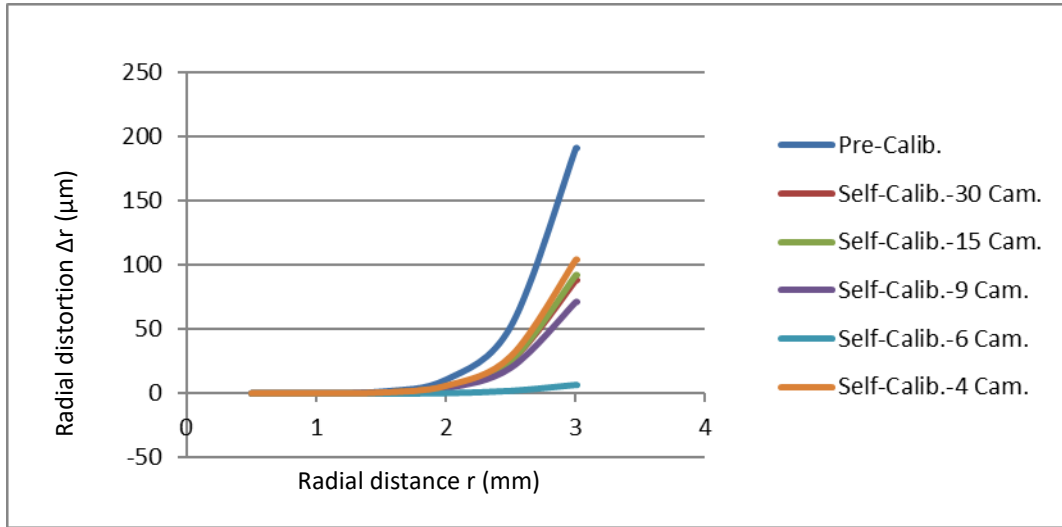

Figure 10. The pre- and self- calibration radial distortions for different number multi-view images

Table 5. The plane surface images and point cloud generation from pre-, self-, and non- calibrated images

Camera (Image)#	Calibration	CP#	RMSE_XYZ (cm)	Sparse point (SP)#	Projection#	Projection#. /SP#	Projection# /Image#
30	Pre-	7	0.76	7054	93235	13.22	3108
	Self-		0.70				
	Non-		24.63				
15	Pre-	7	0.88	7621	54596	7.16	3640
	Self-		0.58				
	Non-		25.60				
9	Pre-	7	1.04	7893	33347	4.22	3705
	Self-		0.59				
	Non-		26.93				
6	Pre-	7	1.02	7375	22876	3.10	3813
	Self-		0.55				
	Non-		27.39				
4	Pre-	7	1.30	6986	15283	2.19	3821
	Self-		0.79				
	Non-		28.69				
2	Pre-	7	1.11	306	612	2.00	306
	Self-		na				
	Non-		7.18				

C. Altuntaş

4. DISCUSSION

The SfM approach photogrammetric evaluation is an easy and simple way to getting image based point cloud data in the absence of pre-calibration parameters. However the measurements are in low accuracy without the camera calibration. The camera's intrinsic and distortion parameters must be known for high accuracy measurement. The focal length has big effects on the accuracy individually. It is achieved from header of the image file for non-metric images or arbitrary value to an imagery evaluation. The camera calibration parameters are attained from pre- or self- calibration. The pre-calibration raises labour and time requirement in photogrammetric measurement. At this time, the self-calibration can be performed for fast and low cost measurement. But the convergent imaging or enough number of projections for plane surface should be considered for high level accuracy of self-camera calibration and executed photogrammetric measurement of multi-view images. The correct pre-calibration is also performed with these image configurations. Nowadays, all the software packages use SfM algorithm, and can perform self-calibration together with estimation the object coordinates of conjugate points.

The self-calibration needs huge computation that forces to computer capacity. Its execution is very hard by the manually selected conjugated object points. However, the image based measurement and camera calibration can be automatically performed by using SfM approach. The object feature points are detected from overlapping images and then they are matched by their similarities in SfM flowchart. The E matrix is used to finding the possible match points using the co-planarity constraint of the overlapping images when the calibration parameters are known, and F matrix is used otherwise.

The self-calibration requires multi-view images to estimate the camera's intrinsic and distortion parameters. The convergent image geometry ensures high accuracy for self-calibration. If the multiple image geometry is retired from convergence imaging, the calibration accuracy will be reduced (Table 2, Figure 8). On the other hand, depending to the measured object geometry such as building, loop close imaging should be performed for high accuracy of the measurement and self-calibration (Table 3). Another issue on the self-calibration is the number of projections and related images. The projection depicts that how many images are connected to a point which a member of the sparse point cloud, and therefore related to number of images. More projections mean high accuracy for image based point cloud and also self-calibration (Table 4, Figure 10). The results of the study indicate that the multi-view evaluation with self-calibration has better or similar level accuracy with respect to pre-calibration when the projection-to-sparse point cloud ratio is more than ten (Table 5).

The previous studies in the literature are presented the potential of consumer-grade digital cameras to maintain their internal geometry in terms of temporal stability and manufacturing consistency [19]. Nevertheless, the camera can be subject of forces that cause to deformation of internal geometry eventually. Thus the self-calibration photogrammetry is guaranty a high accuracy in the measurement under the condition that the imaging geometry is not far away from the proper one.

The computation time for point cloud generation and self-calibration is usually very short. It is depending to image number and computer configurations. In this study, maximum image number (50 images) were processed at 3 minutes 57 seconds by a computer which has 3.10GHz CPU and 8 GB Ram.

5. CONCLUSION

The wide spectrum of applications in close range photogrammetry entails the image acquisition of more complex network geometry with a much lower standardization. The pre-calibration ensures acceptable level accuracy in measurement. It necessitates proper test field, imaging and computation before the photogrammetry evaluation. In addition the camera individual calibration should be performed in particular time periods for checking the stabilization of the camera parameters. On the other hand, high accuracy measurement can be performed with the self-calibration of proper imaging which has convergence or high projections in SfM based point cloud generation. The self-calibration was performed with high accuracy by using loop-close images. However loop close imaging may not possible for every measurement conditions. Thus the images should be convergent as far as possible, or projection-to-sparse point cloud ratio must be raised. Here, projection-to-sparse point cloud ratio of 13.22 created high accuracy to self-calibration. The consumer-grade digital cameras can be used with self-calibration for metric measurement of photogrammetry. For this, the camera intrinsic parameters of non-metric images must be estimated together with point cloud generation by using the SfM algorithm. The non-metric images cause decrease to accuracy on measurement of photogrammetric point cloud.

REFERENCES

[1]   N. Micheletti, J. H. Chandler,, and S. N. Lane, "Structure from motion (SFM) photogram-metry." In: Clarke LE, Nield JM (Eds.) Geomorphological Techniques (Online Edi-tion), https://dspace.lboro.ac.uk/ dspace-jspui/bitstream/2134/17493/3/2.2.2_sfm.pdf, [Access:3 January 2018] (ISSN:2047-0371), 2015

[2]   F. He, T. Zhou, W. Xiong, S. M. Hasheminnasab, and A. Habib, "Automated aerial triangulation for UAV-based mapping," *Remote Sensing*, vol. 10, no. 12, 1952, 2018.

[3]   D. Akca, and A. Gruen, "Comparative geometric and radiometric evaluation of mobile phone and still video cameras," *The Photogrammetric Record*, vol. 24, no. 127, pp. 217–245, 2009.

[4]   S. M. Hasheminasab, T. Zhou, and A. Habib, "GNSS/INS-assisted structure from motion strategies for UAV-based imagery over mechanized agricultural fields," *Remote Sensing*, vol. 12, no. 3, 351, 2020.

[5]   F. Schaffalitzky, and A. Zisserman, Multi-view matching for unordered image sets, or how do I organize my holiday snaps?," ECCV 2002, Part I. LNCS 2350, *Springer, Heidelberg*, 2002.

[6]   M. Calonder, V. Lepetit, C. Strecha, and P. Fua, "BRIEF: binary robust independent elementary features," ECCV 2010, LNCS 6314, *Springer, Berlin Heidelberg*, 2010.

[7]   J. Salvi, X. Armangu, and J. Bat, "A comparative review of camera calibrating methods with accuracy evaluation," *Pattern Recognition*, vol. 35, no. 7, pp. 1617–1635, 2002.

[8]   C. S. Fraser, "Automatic camera calibration in close range photogrammetry," PE&RS, vol. 79, no. 4, pp. 381–388, 2013.

[9]   R. Hartley, and A. Zisserman, "Multiple View Geometry in Computer Vision," Second Edition, *Cambridge University Press,* 2004.

[10] D. Griffiths, and H. Burningham, "Comparison of pre-and self-calibrated camera calibration models for UAS-derived nadir imagery for a SfM application," *Progress in Physical Geography: Earth and Environment*, vol. 43, no. 2, pp. 215-235, 2019.

[11] S. Amelio, and M. L. Brutto, "Close range photogrammetry for measurement of paintings surface deformations," *International Archives of Photogrammetry, Remote Sensing and Spatial Information Sciences*, vol. XXXVIII-5/W1, pp. 1–6, 2009.

[12] M. Scaioni, T. Feng, P. Lu, G. Qiao, X. Tong, R. Li, L. Barazzetti, M. Previtali, and R. Roncellaet, "Close-range photogrammetric techniques for deformation measurement: Applications to landslides," In: Scaioni M (eds) Modern Technologies for Landslide Monitoring and Prediction. *Springer Natural Hazards. Springer, Berlin, Heidelberg*, 2015.

[13] T. Luhmann, "Close range photogrammetry for industrial applications," *ISPRS Journal of Photogrammetry and Remote Sensing*, vol. 65, no. 6, pp. 558-569, 2010.

[14] S. Lee, J. Kim, C. Jin, S. Bae, and C. Choi, "Assesment of smartphone-based technology for remote environmental monitoring and its development," *Instrumentation Science and Technology*, vol. 40, no. 6, pp. 504-529, 2012.

[15] L. D. Desmon, and P. G. Bryan, "Recording architecture at the archaeological site of Uxmal, Mexico: A historical and contemporary view," *Photogrammetric Record*, vol. 18, no. 102, pp. 105-130, 2003.

[16] A. Grün, F. Remondino, and L. Zhang, "Photogrammetric reconstruction of The Great Budha of Baminyan, Afghanistan," *Photogrammetric Record*, vol. 19, no. 107, pp. 177-199, 2004.

[17] S. Cronk, C. Fraser, and H. Hanley, "Automated metric calibration of colour digital cameras," *The Photogrammetric Record*, vol. 21, no. 116, pp. 355–372, 2006.

[18] T. Labe, and W. Förstner,"Geometric stability of low-cost digital consumer cameras," *Int. Archives of Photogrammetry, Remote Sensing and Spatial Information Sciences*, vol. 35/5, part (B), pp. 528-535, 2004.

[19] R. Wackrow, J. H. Chandler, and P. Bryan, "Geometric consistency and stability of consumer-grade digital cameras for accurate spatial measurement," *The Photogrammetric Record*, vol. 22, no. 118, pp. 121–134, 2007.

[20] F. Remondino, and C. Fraser, "Digital camera calibration methods: considerations and comparisons," *Int. Archives of Photogrammetry, Remote Sensing and Spatial Information Sciences*, vol. XXXVI, part 5, pp. 266-272, 2006.

[21] E. L. Hall, J. B. K. Tio, C. A. McPherson, and F. A. Sadjadi, "Measuring curved surfaces for robot vision," *IEEE Computer*, vol. 15, no. 12, pp. 42–54, 1982.

[22] O. D. Faugeras, and G. Toscani, "The calibration problem for stereo," Proceedings of the IEEE Computer Vision and Pattern Recognition, Miami Beach FL, pp. 15–20, 1986.

[23] J. Wang, F. Shi, J. Zhang, and Y. Liu, "A new calibration model of camera lens distortion," *Pattern Recognition*, vol. 41, pp. 607–615, 2008.

[24] J. Sun, X. Chen, Z. Gong, Z. Liu, and Y. Zhao, "Accurate camera calibration with distortion models using sphere images," *Optics and Laser Technology*, vol. 65, pp. 83-87, 2015.

[25] R. Y. Tsai, "A versatile camera calibration technique for high-accuracy 3D machine vision metrology using off-the shelf TV cameras and lenses," *IEEE International Journal Robotics and Automation*, vol. RA-3, no. 4, pp. 323–344, 1987.

[26] G. Q. Wei, and S. D. Ma, "Implicit and explicit camera calibration: Theory and experiments," *IEEE Transactions on Pattern Analysis and Machine Intelligence*, vol. 16, no. 5, pp. 469–480, 1994.

[27] J. Weng, P. Cohen, and M. Herniou, "Camera calibration with distortion models and accuracy evaluation," *IEEE Transactions on Pattern Analysis and Machine Intelligence*, vol. 14, pp. 965–980, 1992.

C. Altuntaş

[28] P. Fasogbon, L. Duvieubourg, and L. Macaire, "Scheimpflug Camera Calibration Using Lens Distortion Model," In: Raman B., Kumar S., Roy P., Sen D. (eds) Proceedings of International Conference on Computer Vision and Image Processing. Advances in Intelligent Systems and Computing, Springer, Singapore, vol 459, doi:10.1007/978-981-10-2104-6_15, 2017.

[29] Y. Chen, H. Ip, Z. Huang, and G. Wang, "Full Camera Calibration from a Single View of Planar Scene." In: Bebis G. et al. (eds) Advances in Visual Computing. ISVC 2008. Lecture Notes in Computer Science, Springer, Berlin, Heidelberg, vol 5358, doi:10.1007/978-3-540-89639-5_78, 2008.

[30] M. E. Amestoy, and O. F. Ortiz, "Global Positioning from a Single Image of a Rectangle in Conical Perspective," *Sensors*, vol. 19, no. 24, 5432, 2019.

[31] F. Bukhari, and M. Dailey, "Robust Radial Distortion from a Single Image", In: Bebis G. et al. (eds) Advances in Visual Computing. ISVC 2010. Lecture Notes in Computer Science, Springer, Berlin, Heidelberg, vol 6454, doi:10.1007/978-3-642-17274-8_2, 2010.

[32] J. Fryer, and D. Brown, "Lens distortion for close-range photogrammetry," *PE&RS*, vol. 52, no. 1, pp. 51-58, 1986.

[33] R. Wang, G. Jiang, L. Quan, and C. Wu, "Camera calibration using lengths of corresponding line segments," *IEEE Xplore*, 11705338, 2010.

[34] M. Mozerov, A. Amato, M. Al-Haj, and J. Gonzalez, "A Simple Method of Multiple Camera Calibration for the Joint Top View Projection," In: Kurzynski M., Puchala E., Wozniak M., Zolnierek A. (eds) Computer Recognition Systems 2. Advances in Soft Computing, vol 45. Springer, Berlin, Heidelberg, doi:10.1007/978-3-540-75175-5_21, 2007.

[35] H. T. Chen, "Geometry-Based Camera Calibration Using Five-Point Correspondences From a Single Image," *IEEE Transactions on Circuits and systems for Video Technology*, vol. 27, no. 12, pp. 2555-2566, 2017.

[36] Y. Civera, D. R. Bueno, A. J. Davison, and J. M. M. Montiel, "Camera self-calibration for sequential Bayesian structure from motion," *IEEE Xplore*, pp. 3411-3416, doi: 10.1109/ROBOT.2009.5152719, 2009.

[37] Y. Furukawa, and J. Ponce, "Accurate camera calibration from multi-view stereo and bundle adjustment," *International Journal of Computer Vision*, vol. 84, pp. 257-268, 2009.

[38] E. Ito, and T. Okatani, "Self-calibration-based approach to critical motion sequences of rolling-shutter structure from motion," *IEEE Xplore*, 17363558, pp. 4512-4520, 2017.

[39] C. S. Fraser, "Digital camera self-calibration," *ISPRS Journal of Photogrammetry and Remote Sensing*, vol. 52, no. 4, pp. 149-159, 1997.

[40] C. Ressl, "Geometry, constraints and computation of the trifocal tensor," PhD Thesis, Reviewer: W. Förstner, H. Pottmann; Institut für Photogrammetrie und Fernerkundung, 2003.

[41] D. G. Lowe, "Distinctive image features from scale-invariant keypoints," *International Journal of Computer Vision*, vol. 60, no. 2, pp. 91-110, 2004.